

Disorder in dissipation-induced topological states: Evidence for a different type of localization transition

Alon Beck and Moshe Goldstein

Raymond and Beverly Sackler School of Physics and Astronomy, Tel Aviv University, Tel Aviv 6997801, Israel

(Dated: August 17, 2021)

The quest for nonequilibrium quantum phase transitions is often hampered by the tendency of driving and dissipation to give rise to an effective temperature, resulting in classical behavior. Could this be different when the dissipation is engineered to drive the system into a nontrivial quantum coherent steady state? In this work we shed light on this issue by studying the effect of disorder on recently-introduced dissipation-induced Chern topological states, and examining the eigenmodes of the Hermitian steady state density matrix or entanglement Hamiltonian. We find that, similarly to equilibrium, each Landau band has a single delocalized level near its center. However, using three different finite size scaling methods we show that the critical exponent ν describing the divergence of the localization length upon approaching the delocalized state is significantly different from equilibrium if disorder is introduced into the non-dissipative part of the dynamics. This indicates a different type of nonequilibrium quantum critical universality class accessible in cold-atom experiments.

Introduction.— Recent years have seen a surge of interest in the driven-dissipative dynamics of quantum many body systems [1, 2]. Of particular interest is the possibility of new nonequilibrium quantum critical phenomena. However, typically far-from-equilibrium conditions give rise to an effective temperature governing the long time physics, and leading to classical criticality. This stands in line with the usual perception of driving and dissipation as causing decoherence and destroying subtle quantum phenomena. This point of view has been challenged by recent works showing how coupling to an environment could be engineered to drive a system towards desired steady states displaying quantum correlations [3–9], such as nonequilibrium topological states [10–23]. In particular, Refs. [18, 19] introduced a protocol, realizable with cold atoms, for purely dissipative dynamics which approaches at a finite rate a mixed steady state as close as desired to a pure topological state. Yet, the resulting topology is encoded in the *Hermitian* steady state density matrix, giving rise to the same topological classes as in equilibrium [10–12, 15, 18, 21, 23–34]. Could this new type of engineered driving still lead to new quantum nonequilibrium criticality?

Every natural system exhibits imperfections and disorder. In equilibrium, it has long been recognized that disorder is actually essential for stabilizing the most basic topological phase, the integer quantum Hall state [35]. Disorder localizes all states in a Landau level except one at energy E_c . The wavefunction localization length diverges as one approaches it as [36, 37]

$$\xi(E) \sim |E - E_c|^{-\nu}, \quad (1)$$

with a critical exponent ν governing the plateau transition. Lately, a debate arose regarding the theoretical value of ν [38–49], and its relation to experiment [50–52]; the currently accepted value is 2.5–2.6.

In this work we study the interplay between disorder and the recipe of Refs. [18, 19] for dissipatively-inducing Chern-insulator states, through the effects of disorder on

the eigenmodes of the steady-state density matrix, which is experimentally measurable in cold atoms [53–57]. This is thus a *Hermitian* localization problem, unrelated to disordered nonhermitian Hamiltonians [58, 59]. We show that disorder in the system-bath coupling leads to the same universality class as in equilibrium, while disorder perturbing the system Hamiltonian is not. We employ three different finite size scaling (FSS) methods, based on (a) the number of conducting states [48, 60]; (b) the local Chern marker [61]; (c) the transfer matrix Lyapunov exponent [37, 47]. The final results are presented in Table II; all methods show that the out-of-equilibrium ν is larger by 0.5–0.6 than equilibrium, hinting at a different universality class.

Recipe.— We now briefly recall the recipe for the dissipative creation of topological states, which is comprehensively described in Ref. [18]. Suppose we have a “reference Hamiltonian”, $H^{\text{ref}} = \sum_{i,j} h_{ij}^{\text{ref}} c_i^\dagger c_j = \sum_\lambda \epsilon_\lambda^{\text{ref}} c_\lambda^\dagger c_\lambda$ (i, j being real space indexes in 2D, and λ an eigenvalue index, which, in the clean case, would correspond to the band number and lattice momentum), with some desired (e.g., topologically-nontrivial) gapped ground state where only low-lying states ($\lambda \leq \lambda_0$) are filled. Rather than implementing H^{ref} as the system Hamiltonian, one may set the system Hamiltonian to zero and employ dissipation to drive the system into a steady-state which is close to the ground state of H^{ref} . For this one takes a system consisting of two types of fermions (e.g., cold atom hyperfine states), with respective creation operators a_i^\dagger (system) and b_i^\dagger (bath). Both fermion species feel a lattice potential in the xy plane, but the bath b -fermions could also escape in the z direction. Besides that, the Hamiltonian of the a -fermions is trivial, ideally featuring no hopping; deviations from this will be described by a system Hamiltonian $H_S = \sum_{i,j} h_{S,ij} a_i^\dagger a_j$. Rather, the dynamics originates from the system-bath coupling Hamiltonian, which is built out of the matrix elements of the reference Hamiltonian. In the rotating frame (with

Method	Equilibrium							Out of equilibrium									
	W	Geometry	L	L_x	N_g	M	L_x^{eff}	W	μ^{eff}	$\frac{\gamma^{\text{in}}}{\gamma^0}$	Geometry	L	L_x	p	N_g	M	L_x^{eff}
I	0.2	$L \times L$	28–63	—	30	53000–740 ^a	—	2	−3.6	0.2	$L \times L$	35–63	—	—	25–31 ^b	32000–290 ^a	—
II	0.2	$L \times L$	21–77	—	—	30000	—	2	−3.6	0.2	$L \times L$	28–77	—	—	—	3000–1500 ^c	—
III	0.2	$L \times L_x$	14–210	$2 \cdot 10^7$	—	5	10^8	5.5	−3.6	0.2	$L \times L_x$	14–49	105	5	—	15000	$1.3 \cdot 10^6$

^a M depends on L [62].

^b $N_g = 25$ for $L \leq 49$ and $N_g = 31$ for $L = 56, 63$.

^c $M = 3000$ for $L \leq 63$ and $M = 1500$ for $L = 70, 77$.

TABLE I. Methods parameters: W is the disorder strength, L and L_x the system size in the y and x directions, respectively, N_g the grid size (method I), M the number of disorder realizations, L_x^{eff} the effective x -length (method III), p the hopping range cutoff (method III, nonequilibrium), μ^{eff} the effective chemical potential, and $\gamma^{\text{in}}/\gamma^0$ the refilling rate in units of $\gamma^0 = 2\pi\nu_0 t^2$.

respect to the system and bath Hamiltonians) it acquires a time-independent form,

$$\begin{aligned}
H_{SB} &= \sum_{i,j} (h_{ij}^{\text{ref}} - \mu^{\text{eff}} \delta_{ij}) b_i^\dagger a_j + \text{h.c.} \\
&= \sum_{\lambda} (\varepsilon_{\lambda}^{\text{ref}} - \mu^{\text{eff}}) b_{\lambda}^\dagger a_{\lambda} + \text{h.c.}, \quad (2)
\end{aligned}$$

where μ^{eff} is an effective “chemical potential”. The utility of the construction now becomes apparent: Suppose the lowest energy band of the reference Hamiltonian is almost flat (dispersionless). By tuning μ^{eff} to its center ($\varepsilon_{\lambda}^{\text{ref}} \approx \mu^{\text{eff}}$ for all $\lambda \leq \lambda_0$), its states becomes *weakly coupled* to the bath compared to states in the other bands, $\lambda > \lambda_0$. Thus, all states are evaporated rapidly, except those belonging to the lowest band. One may then introduce another similar reservoir which refills all trapped states at a uniform rate. Coupling the system to these two reservoirs with different chemical potentials stabilizes a nonequilibrium steady state close to the ground state of the reference Hamiltonian, as we now explain.

Integrating out the baths one gets a Lindblad [63] master equation, from which the Gaussian steady-state ρ can be obtained. The latter is completely characterized by the single-particle density matrix $G_{ij} \equiv \text{tr}(\rho a_i^\dagger a_j)$, which obeys a continuous Lyapunov equation [18, 19, 64]:

$$i[G, h_S^*] + \frac{1}{2} \{G, \gamma^{\text{out}} + \gamma^{\text{in}}\} = \gamma^{\text{in}}, \quad (3)$$

where $\gamma^{\text{in}}, \gamma^{\text{out}}$ are nonnegative Hermitian matrices that describes the rates which particles enter/escape of the system, and h_S^* is the complex conjugate of the matrix h_S . By Fermi’s golden rule, $\gamma_{\lambda}^{\text{out}} = 2\pi\nu_0(\varepsilon_{\lambda}^{\text{ref}} - \mu^{\text{eff}})^2$ is diagonal in the eigenbasis of the reference Hamiltonian [more generally, as a matrix $\gamma^{\text{out}} = 2\pi\nu_0(h^{\text{ref}} - \mu^{\text{eff}}\mathbb{I})^2$, with ν_0 the density of states of the b -species (assumed constant), while γ^{in} is taken as state independent (proportional to the unit matrix). For $h_S = 0$, we can solve Eq. (3) explicitly:

$$G = [1 + \frac{2\pi\nu_0}{\gamma^{\text{in}}}(h^{\text{ref}} - \mu^{\text{eff}}\mathbb{I})^2]^{-1}. \quad (4)$$

We see that G is diagonal in the eigenbasis of H^{ref} , with eigenvalues $n_{\lambda} = \gamma^{\text{in}}/(\gamma^{\text{in}} + \gamma_{\lambda}^{\text{out}})$ representing their

mean occupation. The coupling to two reservoirs with different chemical potentials thus induced a Lorentzian nonequilibrium distribution (in terms of the energies of H^{ref}), unlike the equilibrium Fermi-Dirac distribution. G [or, equivalently, the system-bath entanglement Hamiltonian $-\ln(\rho)$] has a similar band structure to H^{ref} (with the highest occupancy band of G corresponding to the lowest energy band of H^{ref}), which is amenable to topological classification [10–12, 15, 18, 19, 28]. For $\max_{\lambda \leq \lambda_0}(\gamma_{\lambda}^{\text{out}}) \ll \gamma^{\text{in}} \ll \min_{\lambda > \lambda_0}(\gamma_{\lambda}^{\text{out}})$ we get $n_{\lambda \leq \lambda_0} \approx 1$, $n_{\lambda > \lambda_0} \approx 0$, as desired: The steady-state is then close to the ground state of H^{ref} at zero temperature, and will therefore have the same topological index. This motivates the study of the eigenmodes of G and their localization properties in the presence of disorder.

Localization transition.— This work compares the localization quantum phase transition of two systems. The first is the equilibrium Hofstadter model [65] for the integer quantum Hall effect on a square lattice:

$$H_H = t \sum_{r_x, r_y} e^{2\pi i \alpha r_y} a_{r_x+1, r_y}^\dagger a_{r_x, r_y} + a_{r_x, r_y+1}^\dagger a_{r_x, r_y} + \text{h.c.}, \quad (5)$$

where we take $t = 1$, $\alpha = 1/7$. The second system is the out of equilibrium analog, built using the recipe described above [18, 19]: The Hofstadter Hamiltonian (whose lowest band is naturally almost-flat) is taken as the *reference* Hamiltonian $H^{\text{ref}} = H_H$, while $H_S = 0$. To study the localization phase transition we introduce disorder. In equilibrium we add a term $H_D = \sum_{r_x, r_y} w_{r_x, r_y} a_{r_x, r_y}^\dagger a_{r_x, r_y}$, where $w_{r_x, r_y} \in [-W, W]$ are independent and uniformly distributed. Out of equilibrium, there are two options for introducing the same disorder term, realizable in cold atoms using the setup introduced in Refs. [18, 19]: One may either (a) add H_D to H^{ref} while keeping $H_S = 0$, by adding a random component to the laser beam which drives the onsite $a \rightarrow b$ transition in H_{SB} , using, e.g., a speckle pattern [66]; (b) keep $H^{\text{ref}} = H_H$ and set $H_S = H_D$, by adding a random component to the optical lattice potential of the a atoms or to the optical potential confining them to the lattice plane. We find that in both cases the disorder causes a nonequilibrium steady-state localization phase transition of the eigenmodes of G . We can define the localization

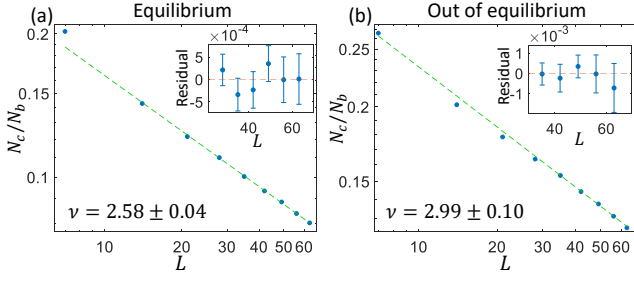


FIG. 1. Log-log plot of $\langle N_c/N_b \rangle$ as function of L (system size), with N_c the number of conducting states and $N_b = \alpha L^2$ ($\alpha = 1/7$) the total number of states per band. Dashed lines represent linear fits with $L \geq 28$ in equilibrium and $L \geq 35$ out of equilibrium. Insets: residual plots.

length of an eigenmode of G by the exponential decay of its envelope, in the same way it is defined for the eigenmodes of H in equilibrium [36, 37]. Similarly to Eq. (1), it behaves as $\xi(n) \propto |n - n_c|^{-\nu}$, where now it depends on the eigenvalue of G , that is, the occupation n (instead of the energy E). n_c is the critical occupation, which replaces the critical energy E_c . In this work we will concentrate on the band of highest occupation, akin to the lowest Landau band in equilibrium [see for example the bottom panel of Fig. 2(b)].

Does ν takes the same value as in equilibrium? In the first case the answer is yes; since $H_S = 0$, G is still given by Eq. (4). Thus, even in the presence of disorder, h^{ref} and G share the *same eigenvectors*, hence the same ν [62]. This argument does not hold in the second scenario (disorder in H_S), since G and h^{ref} have different eigenvectors. Here we need to resort to numerical solution of Eq. (3). We will investigate ν using three FSS methods. For each we first calculate ν in equilibrium (disordered Hofstadter model), and then out of equilibrium ($H^{\text{ref}} = H_H$ and $H_S = H_D$). Again, while in equilibrium we examine the properties of the Hamiltonian (e.g., eigenvector localization length, Chern number), out of equilibrium we investigate the same properties, which are now obtained from G instead of the Hamiltonian. While the band structure in equilibrium depends only on α and the disorder strength W , out of equilibrium it also depends on γ^{in} and μ^{eff} . The results were found not to be sensitive to their particular values, as long as they are chosen so that the disorder broadens the bands more than their clean width but less than their separation [62]. The parameter values are summarized in Table I, and the final results in Table II.

Method I.— Following Ref. [48, 62], we calculate the critical exponent in equilibrium by the scaling of the number of conducting states, N_c ,

$$N_c(L) \propto L^{2-1/\nu}, \quad (6)$$

where L is the system size and ν is the critical exponent. Working with a $L \times L$ Hofstadter model with periodic boundary conditions, we calculate N_c by counting

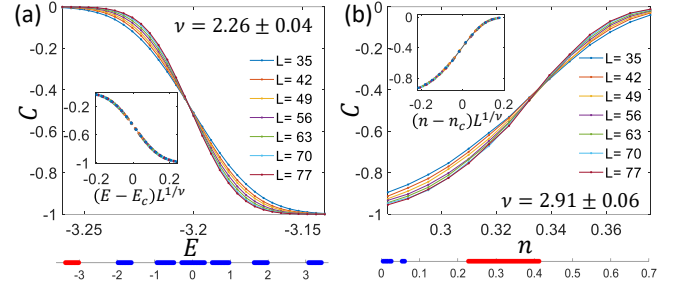


FIG. 2. The average local Chern number (a) in and (b) out of equilibrium. Insets: scaling data collapse. Bottom panels: the seven energy bands in equilibrium, and occupation bands out of equilibrium (note the different scales). The band which is investigated is marked in red and the others in blue.

the number of single-particle states with nonzero Chern number, and average the result over M different disorder realizations. In the presence of disorder, the Chern number can be defined as [67]:

$$C_L(\psi) = -\frac{1}{\pi} \int \text{Im} \langle \partial_{\theta_x} \psi | \partial_{\theta_y} \psi \rangle d\theta_x d\theta_y, \quad (7)$$

where $\psi(\theta_x, \theta_y)$ is the single-particle state and the integral is over the space of twisted periodic boundary conditions, defined by the phases $0 \leq \theta_x, \theta_y \leq 2\pi$. For efficient calculation, we use the method suggested in Ref. [68], employing grid size $N_g \times N_g$ [62]. Corrections to the scaling in Eq. (6) fade quickly with increasing the system size, hence may be ignored by excluding low system sizes. The nonequilibrium generalization is straightforward: We calculate the Chern number of eigenstates of G (instead of H) by introducing the twisted boundary conditions θ_x, θ_y into H^{ref} . Then, we count the conducting states within the highest occupation band. Results are presented in Fig. 1.

Method II.— Here we study FSS of the topological index [36, 62]. In equilibrium, we define the total Chern number $C_L(E)$ as the sum of the Chern numbers defined in Eq. (7) over all single particle states ψ with energy below E (hence it varies between 0 when E is below the lowest band, to -1 when it is in the gap between it and the next band). In the vicinity of the critical energy E_c , it scales as

$$C_L(E) = f((E - E_c)L^{1/\nu}), \quad (8)$$

We note that the transition will be sharp in the thermodynamic limit. For a more efficient estimation of $C_L(E)$, we will use the local Chern marker [61, 69] with open boundary conditions,

$$C(r_x, r_y) = -2\pi i \langle r_x, r_y | \tilde{X} \tilde{Y} - \tilde{Y} \tilde{X} | r_x, r_y \rangle, \quad (9)$$

where \tilde{X}, \tilde{Y} are the projected lattice position operators: $\tilde{X} = P(E)XP(E)$, $\tilde{Y} = P(E)YP(E)$, $P(E)$ being a projection onto states with energy below E . The local

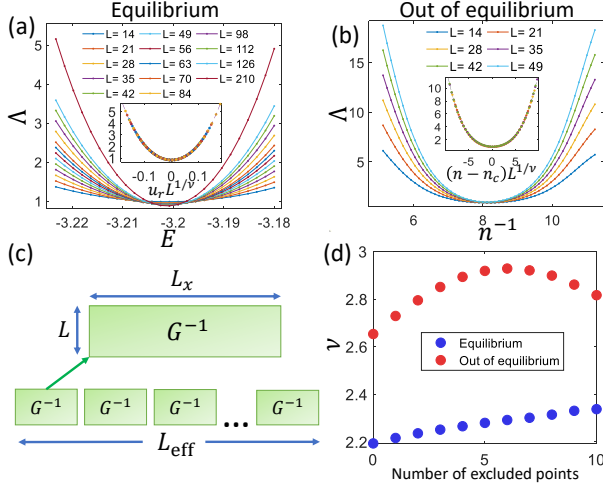


FIG. 3. Dimensionless Lyapunov exponent (a) in and (b) out of equilibrium. Insets: scaling data collapse [in (a) the vertical axis includes corrections to scaling and u_r is the relevant scaling field [62]]. (c) Illustration of the nonequilibrium transfer matrices construction. (d) Comparison of the critical exponent in and out of equilibrium, without corrections to scaling. The horizontal axis represents the number data points that were excluded from each side of the critical point in the chi-squared minimization.

Chern marker fluctuates around the value of the Chern number in the bulk of the system, but takes different values on the edges, so that $\sum_{r_x, r_y} C(r_x, r_y) = 0$. Thus, we average $C(r_x, r_y)$ over the bulk, while excluding $1/4$ of the sample length from each side, $C_L(E) = (4/L^2) \times \sum_{L/4 \leq r_x, r_y \leq 3L/4} C(r_x, r_y)$, and average the result over M different disorder realizations. As in method I, irrelevant corrections exist, but their influence decreases rapidly with increasing system size. We then search for ν , E_c , and the coefficients of a polynomial approximating f [62], which minimize the chi-squared deviation of $C_L(E)$ from the scaling Eq. (8). Out of equilibrium, we calculate $C_L(n)$, the Chern number of eigenstates of G with occupation larger than n , using Eq. (9) with the appropriate projector $P(n)$. The results are presented in Fig. 2.

Method III.— Here we perform FSS of the localization length ξ . Following Ref. [70] (see also [62]), we calculate the localization length with the transfer-matrix method: We consider a long cylinder of size $L_x \times L$, $L_x \gg L$. Let ψ be an eigenvalue of the Hamiltonian with energy E . From the equation $H\psi = E\psi$ we can construct the $2L \times 2L$ transfer-matrix T_{r_x} , defined as:

$$\begin{pmatrix} \psi_{r_x+1} \\ \psi_{r_x} \end{pmatrix} = T_{r_x} \begin{pmatrix} \psi_{r_x} \\ \psi_{r_x-1} \end{pmatrix}, \quad (10)$$

where ψ_{r_x} is a vector with L elements $\psi_{r_x, r_y=1 \dots L}$. Being symplectic, the eigenvalues of each transfer matrix come in reciprocal pairs $\{\lambda, \lambda^{-1}\}$. The same applies to their product, $\mathcal{T} = \prod_{r_x=1}^{L_x} T_{r_x}$. The Lyapunov exponent

(inverse localization length) is defined as:

$$\tilde{\Lambda} \equiv \xi^{-1} = \lim_{L_x \rightarrow \infty} \frac{\ln(\lambda_{\min})}{L_x}, \quad (11)$$

where λ_{\min} is the smallest eigenvalue of \mathcal{T} that is larger than unity. We have applied the Gram-Schmidt process to the columns of \mathcal{T} every 7 multiplications to reduce numerical error. The results are presented in Fig. 3(a). As in the previous method, ν can be extracted by finding a function f that minimize the chi-square of the dimensionless Lyapunov exponent $\Lambda \equiv L\tilde{\Lambda}$. However, since the data contains strong corrections to scaling (typical for the long cylinder geometry), we account for a single irrelevant scaling field [62].

The nonequilibrium generalization from $\Lambda(E)$ to $\Lambda(n)$ is more complicated compared to the previous methods. First, unlike H , G has *non-local hopping terms* which prevent us from constructing a transfer matrix. This requires introducing a cutoff p on the hopping range in the x direction, and setting terms of range larger than p to zero. From this perspective it is advantageous to construct the transfer matrices using G^{-1} , since Eq. (4) shows that for $H_S = 0$ its elements have a finite range $p = 2$. We have verified numerically that the elements of G^{-1} decay exponentially with range for $H_S = H_D$, making truncation at $p = 5$ a very good approximation [62].

A second issue is that in the presence of disorder the structure of G^{-1} can only be obtained numerically, by solving Eq. (3). Thus, we cannot analytically obtain the transfer matrix at a specific x -position, and instead, we can only generate the entire G^{-1} matrix, which is impractical for $L_x \gg 1$. As a solution, we use the scheme depicted in Fig. 3(c): We generate a G^{-1} matrix of size $L_x \times L$ for some large but practical L_x (with periodic boundary conditions) [62]. We repeat this with M disorder realizations, and denote the resulting matrices as $\{(G^{-1})_m\}_{m=1}^M$. From each $(G^{-1})_m$ we extract K transfer matrices ($K = L_x - 2c$, excluding the $c = 7$ matrices closest to each end) by imposing a cutoff p on the hopping range, as explained above. We then define the sequence $\{T_n\}_{n=1}^{MK}$, with $T_{(n-1)K+1}, \dots, T_{nK}$ the transfer matrices extracted from $(G^{-1})_n$. The effective system length is thus $L_{\text{eff}} = MK$. The mismatch between transfer-matrices that originate from different G^{-1} (for example, T_K and T_{K+1}) introduces an error, but it can be reduced by increasing L_x [62].

The results are shown in Fig. 3(b). The numerical effort per sample is still much higher in the nonequilibrium case, limiting our ability to reduce statistical error by either sample averaging or using large system sizes. Hence, we can neither implement corrections to scaling nor drop small systems, and therefore cannot determine ν as accurately as before. We thus resort to extracting the uncorrected nonequilibrium exponent and comparing it with a similarly obtained equilibrium value, to appreciate the significance of their difference, see Fig. 3(d).

Results and Discussion.— The results are summarized in Table II. In equilibrium they are generally in line

Method	I	II	III
Equilibrium	2.58 ± 0.04	2.26 ± 0.04	2.53 ± 0.03
Nonequilibrium	2.99 ± 0.10	2.91 ± 0.06	not convergent, higher than equilibrium

TABLE II. Summary of the results for the critical exponent ν , in and out of equilibrium.

with previous studies [38–49]. For method I, the obtained $\nu = 2.58 \pm 0.04$ is somewhat higher than the value $\nu = 2.50 \pm 0.01$ reported in Ref. [48] (also for $\alpha = 1/7$). This might be related to the fact that there the disorder Hamiltonian has been projected to the clean lowest band. In method II, the result ($\nu = 2.26 \pm 0.04$) is smaller than recent estimates of the critical exponent, which seems to be a general feature of FSS of a topological index [46, 71]. Let us note that in any case we are interested in the equilibrium-nonequilibrium difference, which is larger than this discrepancy. In method III, upon including corrections to scaling we get $\nu = 2.53 \pm 0.03$, $y = 0.44 \pm 0.01$, $\Lambda(E_c) = 0.83 \pm 0.01$, with y the leading irrelevant exponent. This is slightly smaller but still in agreement with $\nu = 2.58 \pm 0.03$ obtained in Ref. [47] for the Hofstadter model.

Out of equilibrium, methods I and II give rise to values which are significantly higher than in equilibrium. The results of method III are not convergent, but they still strongly suggest that ν is higher than equilibrium by 0.5–0.6 (see. Fig. 3(d)), in agreement with the other methods. We have also verified that our results are insensitive to the specific parameter values [62]. All this points at a different type of nonequilibrium universality class.

Let us reiterate that the single-particle density matrix G is Hermitian. Furthermore, G^{-1} is local in space. The locality is exact for $h_S = 0$, where G^{-1} is essentially the square of h^{ref} , see Eq. (4). We have found that for disorder in H_S the elements of G^{-1} have distributions without fat tails, and with averages and correlations which decay exponentially with distance [62]. Thus, our re-

sults indicate a different type of universality class of the local Hermitian disordered G^{-1} , which is rooted in the nonequilibrium nature of the system.

The value of ν could be measured experimentally, by using the following protocol: (i) realize the cold atoms setup described in Ref. [18]; (ii) use a laser speckle [66] to introduce disorder, either in the beam that induce the $a \rightarrow b$ transitions (for disorder in H^{ref}), or in the beam that is responsible for the confinement of the a -atoms (for disorder in H_S), as discussed above; (iii) measure G as demonstrated in Refs. [53–57]; and (iv) repeat for different system sizes to extract ν through FSS.

Conclusions.— In this work we have investigated the effects of disorder on dissipation-induced topological states. We demonstrated the existence of nonequilibrium steady-state localization phase transition similar to the integer quantum Hall plateau transition. Using three FSS methods, we found a significant difference between the value of the critical exponent ν in and out of equilibrium when disorder is introduced into the non-dissipative part of the Lindbladian. This indicates a different type of nonequilibrium quantum universality class, despite the steady state density matrix being Hermitian and local. Our findings could be tested in cold-atom experiments. In the future it would be interesting to investigate other types of disorder (e.g., long range [72–74]), to attack the problem using field theoretical methods [2, 37], and to study the relation between the steady state and the non-hermitian [58, 59, 75] decay towards it (a relation which is nontrivial out of equilibrium [19]), as well as the possibility of new many-body localization transition [76, 77].

ACKNOWLEDGMENTS

We thank I.S. Burmistrov, R. Ilan, and E. Shimshoni for useful discussions. Support by the Israel Science Foundation (Grant No. 227/15) and the US-Israel Binational Science Foundation (Grant No. 2016224) is gratefully acknowledged.

-
- [1] A. Kamenev, *Field Theory of Non-Equilibrium Systems* (Cambridge University Press, 2009).
 - [2] L. M. Sieberer, M. Buchhold, and S. Diehl, Keldysh field theory for driven open quantum systems, *Reports on Progress in Physics* **79**, 096001 (2016).
 - [3] S. Diehl, A. Micheli, A. Kantian, B. Kraus, H. P. Buchler, and P. Zoller, Quantum states and phases in driven open quantum systems with cold atoms, *Nature Physics* **4**, 878 (2008).
 - [4] B. Kraus, H. P. Buchler, S. Diehl, A. Kantian, A. Micheli, and P. Zoller, Preparation of entangled states by quantum markov processes, *Physical Review A* **78**, 042307 (2008).
 - [5] F. Verstraete, M. M. Wolf, and J. I. Cirac, Quantum computation and quantum-state engineering driven by dissipation, *Nature Physics* **5**, 633 (2009).
 - [6] H. Weimer, M. Muller, I. Lesanovsky, P. Zoller, and H. P. Buchler, A Rydberg quantum simulator, *Nature Physics* **6**, 382 (2010).
 - [7] J. Otterbach and M. Lemesko, Dissipative preparation of spatial order in rydberg-dressed bose-einstein condensates, *Physical Review Letters* **113**, 070401 (2014).
 - [8] N. Lang and H. P. Buchler, Exploring quantum phases by driven dissipation, *Physical Review A* **92**, 012128 (2015).
 - [9] L. Zhou, S. Choi, and M. D. Lukin, Symmetry-protected dissipative preparation of matrix product states, arXiv:1706.01995 [quant-ph] (2017).
 - [10] S. Diehl, E. Rico, M. A. Baranov, and P. Zoller, Topology by dissipation in atomic quantum wires, *Nature Physics* **7**, 971 (2011).

- [11] C.-E. Bardyn, M. A. Baranov, E. Rico, A. Imamoglu, P. Zoller, and S. Diehl, Majorana modes in driven-dissipative atomic superfluids with a zero Chern number, *Physical Review Letters* **109**, 130402 (2012).
- [12] C.-E. Bardyn, M. A. Baranov, C. V. Kraus, E. Rico, A. Imamoglu, P. Zoller, and S. Diehl, Topology by dissipation, *New Journal of Physics* **15**, 085001 (2013).
- [13] R. Konig and F. Pastawski, Generating topological order: No speedup by dissipation, *Physical Review B* **90**, 045101 (2014).
- [14] E. Kapit, M. Hafezi, and S. H. Simon, Induced self-stabilization in fractional quantum Hall states of light, *Physical Review X* **4**, 031039 (2014).
- [15] J. C. Budich, P. Zoller, and S. Diehl, Dissipative preparation of Chern insulators, *Physical Review A* **91**, 042117 (2015).
- [16] F. Iemini, D. Rossini, R. Fazio, S. Diehl, and L. Mazza, Dissipative topological superconductors in number-conserving systems, *Physical Review B* **93**, 115113 (2016).
- [17] Z. Gong, S. Higashikawa, and M. Ueda, Zeno Hall effect, *Physical Review Letters* **118**, 200401 (2017).
- [18] M. Goldstein, Dissipation-induced topological insulators: A no-go theorem and a recipe, *SciPost Physics* **7**, 67 (2019).
- [19] G. Shavit and M. Goldstein, Topology by dissipation: Transport properties, *Physical Review B* **101**, 125412 (2020).
- [20] F. Tonielli, J. C. Budich, A. Altland, and S. Diehl, Topological field theory far from equilibrium, *Phys. Rev. Lett.* **124**, 240404 (2020).
- [21] T. Yoshida, K. Kudo, H. Katsura, and Y. Hatsugai, Fate of fractional quantum Hall states in open quantum systems: Characterization of correlated topological states for the full Liouvillian, *Phys. Rev. Research* **2**, 033428 (2020).
- [22] S. Bandyopadhyay and A. Dutta, Dissipative preparation of many-body Floquet Chern insulators, *arXiv:2005.09972 [cond-mat.stat-mech]* (2020).
- [23] A. Altland, M. Fleischhauer, and S. Diehl, Symmetry classes of open fermionic quantum matter, *arXiv:2007.10448 [cond-mat.str-el]* (2020).
- [24] A. Rivas, O. Viyuela, and M. A. Martin-Delgado, Density-matrix Chern insulators: Finite-temperature generalization of topological insulators, *Phys. Rev. B* **88**, 155141 (2013).
- [25] Z. Huang and D. P. Arovas, Topological indices for open and thermal systems via Uhlmann's phase, *Phys. Rev. Lett.* **113**, 076407 (2014).
- [26] O. Viyuela, A. Rivas, and M. A. Martin-Delgado, Two-dimensional density-matrix topological fermionic phases: Topological Uhlmann numbers, *Phys. Rev. Lett.* **113**, 076408 (2014).
- [27] E. P. L. van Nieuwenburg and S. D. Huber, Classification of mixed-state topology in one dimension, *Phys. Rev. B* **90**, 075141 (2014).
- [28] J. C. Budich and S. Diehl, Topology of density matrices, *Phys. Rev. B* **91**, 165140 (2015).
- [29] F. Grusdt, Topological order of mixed states in correlated quantum many-body systems, *Phys. Rev. B* **95**, 075106 (2017).
- [30] C.-E. Bardyn, A recipe for topological observables of density matrices, *arXiv:1711.09735 [cond-mat.quant-gas]* (2017).
- [31] C.-E. Bardyn, L. Wawer, A. Altland, M. Fleischhauer, and S. Diehl, Probing the topology of density matrices, *Phys. Rev. X* **8**, 011035 (2018).
- [32] D.-J. Zhang and J. Gong, Topological characterization of one-dimensional open fermionic systems, *Phys. Rev. A* **98**, 052101 (2018).
- [33] A. Coser and D. Pérez-García, Classification of phases for mixed states via fast dissipative evolution, *Quantum* **3**, 174 (2019).
- [34] S. Lieu, M. McGinley, and N. R. Cooper, Tenfold way for quadratic Lindbladians, *Phys. Rev. Lett.* **124**, 040401 (2020).
- [35] K. v. Klitzing, G. Dorda, and M. Pepper, New method for high-accuracy determination of the fine-structure constant based on quantized Hall resistance, *Phys. Rev. Lett.* **45**, 494 (1980).
- [36] B. Huckestein, Scaling theory of the integer quantum Hall effect, *Reviews of Modern Physics* **67**, 357 (1995).
- [37] F. Evers and A. D. Mirlin, Anderson transitions, *Reviews of Modern Physics* **80**, 1355 (2008).
- [38] K. Slevin and T. Ohtsuki, Critical exponent for the quantum hall transition, *Phys. Rev. B* **80**, 041304 (2009).
- [39] H. Obuse, A. R. Subramaniam, A. Furusaki, I. A. Gruzberg, and A. W. W. Ludwig, Conformal invariance, multifractality, and finite-size scaling at anderson localization transitions in two dimensions, *Physical Review B* **82**, 035309 (2010).
- [40] M. Amado, A. V. Malyshev, A. Sedrakyan, and F. Domínguez-Adame, Numerical study of the localization length critical index in a network model of plateau-plateau transitions in the quantum Hall effect, *Physical Review Letters* **107**, 066402 (2011).
- [41] I. C. Fulga, F. Hassler, A. R. Akhmerov, and C. W. J. Beenakker, Topological quantum number and critical exponent from conductance fluctuations at the quantum Hall plateau transition, *Physical Review B* **84**, 245447 (2011).
- [42] K. Slevin and T. Ohtsuki, Finite size scaling of the Chalker-Coddington model, *International Journal of Modern Physics: Conference Series* **11**, 60 (2012).
- [43] H. Obuse, I. A. Gruzberg, and F. Evers, Finite-size effects and irrelevant corrections to scaling near the integer quantum Hall transition, *Physical Review Letters* **109**, 206804 (2012).
- [44] W. Nuding, A. Klumper, and A. Sedrakyan, Localization length index and subleading corrections in a Chalker-Coddington model: A numerical study, *Physical Review B* **91**, 115107 (2015).
- [45] I. A. Gruzberg, A. Klumper, W. Nuding, and A. Sedrakyan, Geometrically disordered network models, quenched quantum gravity, and critical behavior at quantum Hall plateau transitions, *Physical Review B* **95**, 125414 (2017).
- [46] M. Ippoliti, S. D. Geraedts, and R. N. Bhatt, Integer quantum Hall transition in a fraction of a landau level, *Physical Review B* **97**, 014205 (2018).
- [47] M. Puschmann, P. Cain, M. Schreiber, and T. Vojta, Integer quantum Hall transition on a tight-binding lattice, *Physical Review B* **99**, 121301 (2019).
- [48] Q. Zhu, P. Wu, R. N. Bhatt, and X. Wan, Localization-length exponent in two models of quantum Hall plateau transitions, *Physical Review B* **99**, 024205 (2019).
- [49] B. Sbierski, E. J. Dresselhaus, J. E. Moore, and I. A. Gruzberg, Criticality of two-dimensional disordered dirac

- fermions in the unitary class and universality of the integer quantum hall transition, *Phys. Rev. Lett.* **126**, 076801 (2021).
- [50] W. Li, G. A. Csáthy, D. C. Tsui, L. N. Pfeiffer, and K. W. West, Scaling and universality of integer quantum Hall plateau-to-plateau transitions, *Phys. Rev. Lett.* **94**, 206807 (2005).
 - [51] W. Li, C. L. Vicente, J. S. Xia, W. Pan, D. C. Tsui, L. N. Pfeiffer, and K. W. West, Scaling in plateau-to-plateau transition: A direct connection of quantum Hall systems with the anderson localization model, *Phys. Rev. Lett.* **102**, 216801 (2009).
 - [52] A. J. M. Giesbers, U. Zeitler, L. A. Ponomarenko, R. Yang, K. S. Novoselov, A. K. Geim, and J. C. Maan, Scaling of the quantum Hall plateau-plateau transition in graphene, *Phys. Rev. B* **80**, 241411 (2009).
 - [53] P. Hauke, M. Lewenstein, and A. Eckardt, Tomography of band insulators from quench dynamics, *Phys. Rev. Lett.* **113**, 045303 (2014).
 - [54] N. Fläschner, B. S. Rem, M. Tarnowski, D. Vogel, D.-S. Lühmann, K. Sengstock, and C. Weitenberg, Experimental reconstruction of the berry curvature in a Floquet Bloch band, *Science* **352**, 1091 (2016).
 - [55] M. Tarnowski, M. Nuske, N. Fläschner, B. Rem, D. Vogel, L. Freystatzky, K. Sengstock, L. Mathey, and C. Weitenberg, Observation of topological Bloch-state defects and their merging transition, *Phys. Rev. Lett.* **118**, 240403 (2017).
 - [56] L. A. Peña Ardila, M. Heyl, and A. Eckardt, Measuring the single-particle density matrix for fermions and hard-core bosons in an optical lattice, *Phys. Rev. Lett.* **121**, 260401 (2018).
 - [57] J.-H. Zheng, B. Irsigler, L. Jiang, C. Weitenberg, and W. Hofstetter, Measuring an interaction-induced topological phase transition via the single-particle density matrix, *Phys. Rev. A* **101**, 013631 (2020).
 - [58] N. Hatano and D. R. Nelson, Localization transitions in non-Hermitian quantum mechanics, *Phys. Rev. Lett.* **77**, 570 (1996).
 - [59] Y. Ashida, Z. Gong, and M. Ueda, Non-Hermitian physics, *arXiv:2006.01837 [cond-mat.mes-hall]* (2020).
 - [60] K. Yang and R. N. Bhatt, Floating of extended states and localization transition in a weak magnetic field, *Physical Review Letters* **76**, 1316 (1996).
 - [61] R. Bianco and R. Resta, Mapping topological order in coordinate space, *Physical Review B* **84**, 241106 (2011).
 - [62] See the supplemental material [URL] for technical details.
 - [63] P. Z. Crispin Gardiner, *Quantum Noise* (Springer Berlin Heidelberg, 2004).
 - [64] F. Schwarz, M. Goldstein, A. Dorda, E. Arrigoni, A. Weichselbaum, and J. von Delft, Lindblad-driven discretized leads for nonequilibrium steady-state transport in quantum impurity models: Recovering the continuum limit, *Phys. Rev. B* **94**, 155142 (2016).
 - [65] D. R. Hofstadter, Energy levels and wave functions of Bloch electrons in rational and irrational magnetic fields, *Physical Review B* **14**, 2239 (1976).
 - [66] J. Goodman, *Speckle phenomena in optics : theory and applications* (SPIE Press, Bellingham, Washington, 2020).
 - [67] Q. Niu, D. J. Thouless, and Y.-S. Wu, Quantized Hall conductance as a topological invariant, *Physical Review B* **31**, 3372 (1985).
 - [68] T. Fukui, Y. Hatsugai, and H. Suzuki, Chern numbers in discretized Brillouin zone: Efficient method of computing (spin) Hall conductances, *Journal of the Physical Society of Japan* **74**, 1674 (2005).
 - [69] M. D. Caio, G. Moller, N. R. Cooper, and M. J. Bhaseen, Topological marker currents in Chern insulators, *Nature Physics* **15**, 257 (2019).
 - [70] A. MacKinnon and B. Kramer, The scaling theory of electrons in disordered solids: Additional numerical results, *Zeitschrift fur Physik B Condensed Matter* **53**, 1 (1983).
 - [71] T. A. Loring and M. B. Hastings, Disordered topological insulators via C*-algebras, *EPL (Europhysics Letters)* **92**, 67004 (2010).
 - [72] M. M. Fogler, A. Y. Dobin, and B. I. Shklovskii, Localization length at the resistivity minima of the quantum hall effect, *Phys. Rev. B* **57**, 4614 (1998).
 - [73] P. M. Ostrovsky, I. V. Gornyi, and A. D. Mirlin, Quantum criticality and minimal conductivity in graphene with long-range disorder, *Phys. Rev. Lett.* **98**, 256801 (2007).
 - [74] A. Rycerz, J. Tworzydło, and C. W. J. Beenakker, Anomalously large conductance fluctuations in weakly disordered graphene, *Europhysics Letters (EPL)* **79**, 57003 (2007).
 - [75] N. Silberstein, J. Behrends, M. Goldstein, and R. Ilan, Berry connection induced anomalous wave-packet dynamics in non-Hermitian systems, *arXiv:2004.13746 [cond-mat.mes-hall]* (2020).
 - [76] R. Nandkishore and D. A. Huse, Many-body localization and thermalization in quantum statistical mechanics, *Annual Review of Condensed Matter Physics* **6**, 15 (2015).
 - [77] E. Altman and R. Vosk, Universal dynamics and renormalization in many-body-localized systems, *Annual Review of Condensed Matter Physics* **6**, 383 (2015).

SUPPLEMENTAL MATERIAL FOR: “DISORDER IN DISSIPATION-INDUCED TOPOLOGICAL STATES: EVIDENCE FOR A DIFFERENT TYPE OF LOCALIZATION TRANSITION”

In this Supplemental Material we provide additional technical details and results. In Sec. S.I we display an argument to the fact that when the disorder appears in the system-bath coupling Hamiltonian, the localization phase transition is in the same universality class as in equilibrium. In Secs. S.II–S.IV we present additional details regarding the three methods which were used to calculate the critical exponent ν out of equilibrium. In Sec. S.V we discuss the choice of parameters and verify that the critical exponent is universal, i.e., independent of the exact parameter values. Finally, in Sec. S.VI we characterize the distribution and correlation of the elements of the matrix G^{-1} .

S.I. DISORDER IN THE DISSIPATIVE DYNAMICS

In the main text we have stated that if we consider disorder only in the reference Hamiltonian h^{ref} (that is, the dynamics is purely-dissipative, $H_S = 0$), then the critical exponent of the phase transition is the same as in equilibrium (that is, in the same universality class). We now present a more detailed argument for this. In fact, it is a special case of the following claim:

Claim. Let h be a nondegenerate Hamiltonian with a property $\xi_h(E)$, which is a function of the eigenstates of h (with energy E). Suppose we have a phase transition described by a scaling law, $\xi_h(E) \propto |E - E_c|^{-\nu}$, where E_c is the critical energy and ν is the critical exponent. Then, any analytic function $G = g(h)$ of h that satisfies

$$0 < \left. \frac{dg}{dh} \right|_{E_c} < \infty, \quad (\text{S1})$$

will display a phase transition with the same critical exponent. That is, $\xi_G(n) \propto |n - n_c|^{-\nu}$, where n represent an eigenvalue of G .

Proof. We notice that G has the same eigenstates as h , but with different eigenvalues described by the relation $n(E) = g(E)$, where $n(E)$ is the eigenvalue of G corresponding to the eigenvalue E of h . Since ξ is determined only by the eigenstates, we have

$$\xi_G(n(E)) = \xi_h(E), \quad (\text{S2})$$

and thus

$$\xi_G(n) \propto |E - E_c|^{-\nu} = |g^{-1}(n) - g^{-1}(n_c)|^{-\nu}, \quad (\text{S3})$$

where g^{-1} is the inverse of the function g . We note that g^{-1} is well defined around n_c since $0 < \left. \frac{dg}{dh} \right|_{E_c} < \infty$. Expanding g^{-1} to first order around n_c , we get

$$\xi_G(n) \approx \left| \left. \frac{dg^{-1}}{dn} \right|_{n_c} (n - n_c) \right|^{-\nu}, \quad (\text{S4})$$

hence $\xi(n) \propto |n - n_c|^{-\nu}$, as expected.

Going back to our case, Eq. (5) of the main text shows that for $H_S = 0$ the single-particle density matrix G can be expressed as a function of h^{ref} , whose derivative is

$$\frac{dG}{dh^{\text{ref}}} = -G^2 \frac{2\pi\nu_0}{\gamma_{\text{in}}} 2(h^{\text{ref}} - \mu^{\text{eff}}), \quad (\text{S5})$$

that is, condition (S1) will be satisfied for $\mu^{\text{eff}} \neq E_c$.

S.II. ADDITIONAL DETAILS FOR METHOD I

Calculation of the Chern number. For efficient calculation of the Chern number we have followed the method of Ref. [68]. We divide the parameter space $0 \leq \theta_x, \theta_y \leq 2\pi$ into a grid of size $N_g \times N_g$ with equal spacing. For each point,

$$\boldsymbol{\theta} = (\theta_x, \theta_y) = \frac{2\pi}{N_g} (r_x, r_y), \quad r_x, r_y = 0, \dots, N_g - 1, \quad (\text{S6})$$

Equilibrium			Out of equilibrium		
L_{\min}	ν	χ_{red}^2	L_{\min}	ν	χ_{red}^2
7	2.36 ± 0.01	46.4	7	3.00 ± 0.01	18
14	2.61 ± 0.02	0.92	14	3.26 ± 0.03	1.2
21	2.63 ± 0.03	0.94	21	3.22 ± 0.05	1.2
28	2.58 ± 0.04	0.57	28	3.15 ± 0.06	1.0
35	2.64 ± 0.07	0.32	35	2.99 ± 0.10	0.28
42	2.62 ± 0.12	0.46	42	2.97 ± 0.19	0.41

TABLE ST1. The results of the critical exponent ν without correction to scaling, extracted from fits of the number of conducting states, Eq. (S10). The smallest system size is taken as L_{\min} and the largest system size is always $L_{\max} = 63$.

we define:

$$U_{\hat{\mu}}(\boldsymbol{\theta}) \equiv \langle \psi(\boldsymbol{\theta}) | \psi(\boldsymbol{\theta} + \hat{\mu}) \rangle / N_{\hat{\mu}}(\boldsymbol{\theta}), \quad (\text{S7})$$

where $N_{\hat{\mu}}(\boldsymbol{\theta}) \equiv |\langle \psi(\boldsymbol{\theta}) | \psi(\boldsymbol{\theta} + \hat{\mu}) \rangle|$ is a normalization factor, and $\hat{\mu} = \hat{x}, \hat{y}$ is a grid lattice vector in the x or y direction, respectively. We define a discretized version of the Berry curvature,

$$F(\boldsymbol{\theta}) \equiv \ln [U_x(\boldsymbol{\theta})U_y(\boldsymbol{\theta} + \hat{x})U_x(\boldsymbol{\theta} + \hat{y})^{-1}U_y(\boldsymbol{\theta})^{-1}], \quad (\text{S8})$$

where the principal branch of the logarithm is used. Finally, the Chern number is defined as

$$C \equiv \frac{1}{2\pi i} \sum_{\boldsymbol{\theta}} F(\boldsymbol{\theta}), \quad (\text{S9})$$

which must result in an integer value. However, the result might contain an error if N_g is not large enough. In our case we can detect errors by checking that the sum of the Chern numbers of all the single-particle states equals -1 (the total Chern number of the first Landau band). If the result is different than -1 , we know that at least one error has occurred in the calculation and therefore reject it. We have taken values of N_g which would keep the rejection rate smaller than 2%: In equilibrium, we choose $N_g = 30$ for all of the system sizes. Out of equilibrium, we choose $N_g = 25$ for $L = 7, \dots, 49$, and $N_g = 31$ for $L = 56, 63$.

Calculation of the critical exponent. Unlike an infinite system, in which an extended (conducting) state exists only at a single energy E_c , in a finite-sized system there is a range of extended states, corresponding to the range of energies with localization lengths $\xi(E) > L$. Thus, to obtain the finite-size mobility edges need to solve $\xi(E) = \xi_0 |E - E_c|^{-\nu} = L$, leading to $E_{1,2} = E_c \pm (\xi_0/L)^{1/\nu}$. Therefore, the number of conducting states would be $N_c = L^2 \int_{E_1}^{E_2} \rho(E) dE$, where $\rho(E)$ is the density of states of the band. Approximating $\rho(E) \approx \rho(E_c)$ and recalling that the total number of states in a Landau band is $N_b = \alpha L^2$ ($\alpha = 1/7$), we obtain the scaling relation

$$\frac{N_c}{N_b} = a L^{-1/\nu}, \quad (\text{S10})$$

where a is some constant. ν can be extracted by numerical calculations of N_c for different system sizes. The results (without corrections to scaling) in and out of equilibrium are presented in Table ST1. In equilibrium, the corrections to scaling are significant only when $L_{\min} = 7$. The first correction can be included by considering the generalized scaling form:

$$\frac{N_c}{N_b} = a (1 + b L^{-y}) L^{-1/\nu}, \quad (\text{S11})$$

where $y > 0$ is the leading irrelevant exponent. We managed to consistently include corrections to scaling only when the lowest system size is included (that is, $L = 7, \dots, 63$). This leads to $\nu = 2.63 \pm 0.02$, $y = 4.6 \pm 0.71$, $\chi_{\text{red}}^2 = 0.99$, which is in agreement with the values obtained without corrections to scaling but with the lower system sizes being excluded (as described below). Out of equilibrium, a single correction to scaling in the form of Eq. (S11) is not compatible with the data even when the lowest system size is included. Therefore, we base our final result only on fits without corrections to scaling with the lower system sizes excluded. The lowest included system size was chosen as $L_{\min} = 28$ in equilibrium and $L_{\min} = 35$ out of equilibrium. This choice ensures that the three lowest system sizes are excluded to avoid corrections to scaling, but also that the change in ν between the employed L_{\min} and using the following value $L_{\min} + 1/\alpha = L_{\min} + 7$ is smaller than the uncertainty in ν .

Equilibrium			Out of equilibrium		
L_{\min}	ν	χ_{red}^2	L_{\min}	ν	χ_{red}^2
7	2.410 ± 0.007	3.5	7	3.65 ± 0.01	25
14	2.42 ± 0.01	3.2	14	3.91 ± 0.03	1.7
21	2.41 ± 0.01	3.8	21	3.86 ± 0.04	1.8
28	2.39 ± 0.02	4.4	28	3.77 ± 0.05	0.67
35	2.43 ± 0.03	5.1	35	3.68 ± 0.09	0.45
42	2.52 ± 0.06	6.4	42	3.57 ± 0.15	0.34

TABLE ST2. The results of the critical exponent ν without correction to scaling, extracted from fits of the width of conducting states density, ΔE_c [cf. Eq. (S12)]. The smallest system size is taken as L_{\min} and the largest system size is always $L_{\max} = 63$.

An additional way for extracting the critical exponent is by looking at the width of the density of the conducting states, $\rho_c(E)$, defined as

$$\Delta E_c^2 = \frac{L^2}{N_c} \int \rho_c(E) E^2 dE - \left[\frac{L^2}{N_c} \int \rho_c(E) E dE \right]^2, \quad (\text{S12})$$

which is expected to scale as $\Delta E_c \sim L^{-1/\nu}$. The results without corrections are presented in Table ST2. While they also suggest a higher value of the critical exponent out of equilibrium, they seem to be less reliable than the results with the number of conducting states, as evidenced by the significantly large chi-squared values. This may imply that the width of the distribution is more sensitive to finite-size corrections than the number of conducting states (See the discussion around Fig. 7 of Ref. [48]).

S.III. ADDITIONAL DETAILS FOR METHOD II

The results of the local Chern marker calculations are presented in Fig. SF1. Corrections to scaling are present at low system sizes. This can be seen in the insets, which show that the low systems sizes curves cross the large system curves away from E_c . The corrections to scaling for small system sizes turn out to be difficult to fit accurately. However, they also decrease rapidly with increasing system sizes. We therefore resort to omitting smaller system sizes and ignoring corrections to scaling. We note that the result also depends on the range of energies (or occupations out of equilibrium) that were included in the fit. Therefore, we chose a range of energies (occupations) in which the result is most stable (least sensitive to increasing or decreasing the number of included points). For example, for $L_{\min} = 35$ we have estimated $\nu = 2.26 \pm 0.04$ from the results presented in Fig. SF2(a). As for the degree D of the polynomial $f(x) = \sum_{q=0}^D a_q x^q$ that was used to approximate the scaling function f , we have verified that it is large enough to capture the behavior in the given range, but is not too large, so as to prevent overfitting. We have thus used $D = 5$ in equilibrium and $D = 7$ out of equilibrium. The results in and out of equilibrium are shown in Table ST3. In order to avoid correction to scaling effects, we have chosen to exclude the four first system sizes. That is, the lowest included system size was chosen as $L_{\min} = 35$ in and out of equilibrium. As in method I, we also verified that the change in ν with respect to using the following value $L_{\min} + 1/\alpha = L_{\min} + 7$ is smaller than the uncertainty in ν .

To verify these results, we have also extracted the critical exponent from the L -dependence of the derivative of C

Equilibrium			Out of equilibrium		
L_{\min}	ν	χ_{red}^2	L_{\min}	ν	χ_{red}^2
14	2.28 ± 0.06	40.2	14	2.81 ± 0.04	25
21	2.23 ± 0.05	17.4	21	2.79 ± 0.06	12
28	2.24 ± 0.05	8.3	28	2.87 ± 0.07	5.4
35	2.26 ± 0.04	5.6	35	2.91 ± 0.06	3.5
42	2.26 ± 0.04	6.1	42	2.92 ± 0.08	4
49	2.20 ± 0.05	5.3	49	2.89 ± 0.10	4

TABLE ST3. The results of the critical exponent ν , extracted from method II. The smallest system size is taken as L_{\min} and the largest system size is always $L_{\max} = 77$.

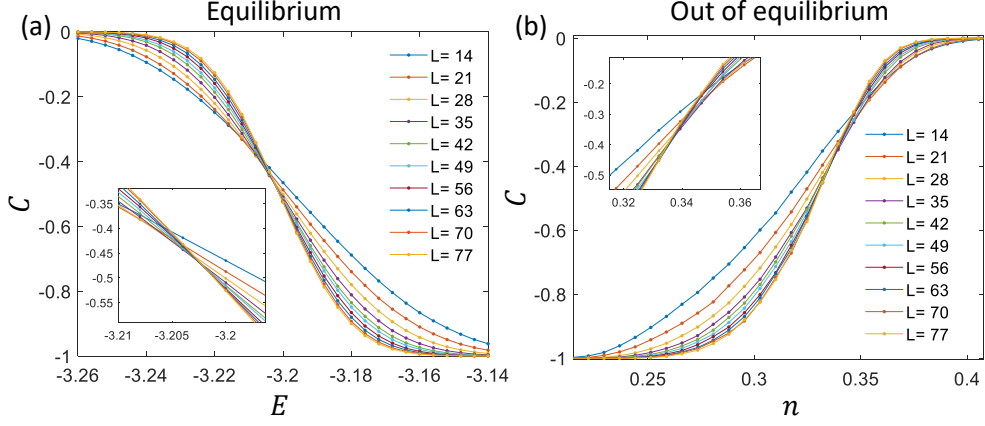


FIG. SF1. The local Chern marker for system sizes $L = 14, \dots, 77$, (a) in equilibrium (results averaged over $3 \cdot 10^4$ disorder realizations); (b) out of equilibrium (results averaged over $3 \cdot 10^3$ disorder realizations). Inset: zoom-in onto the vicinity of the critical point. We note that the data presented here includes all the data from Fig. 2 in the main text, and in addition data for smaller system sizes. This allows to see more clearly the existence of corrections to scaling in the lower system sizes.

at the critical point. For example, in equilibrium, since $C_L(E) = f\left((E - E_c)L^{\frac{1}{\nu}}\right)$, we have

$$\ln\left(\left.\frac{\partial C_L(E)}{\partial E}\right|_{E_c}\right) = \ln(f'(0)) + \frac{1}{\nu} \ln(L). \quad (\text{S13})$$

By fitting a polynomial expansion to each $C_L(E)$ data set at fixed L , we can obtain the left hand side of the last equation by approximating $\left.\frac{\partial C_L(E)}{\partial E}\right|_{E_c} \approx \max\left(\frac{\partial C_L(E)}{\partial E}\right)$. Then, ν can be extracted from a linear fit of the logarithm of the latter quantity as function of $\ln(L)$. While we found this method to be less stable, its results were still in agreement with the chi-square minimization results: In equilibrium we got $\nu \approx 2.2 - 2.3$, while out of equilibrium we got $\nu \approx 2.8 - 3.1$.

S.IV. ADDITIONAL DETAILS FOR METHOD III

Equilibrium. As we mentioned in the main text, in Method III corrections to scaling need to be taken into account, as can be seen from the L dependence of the minima in Fig. SF3. We note that unlike the two previous methods,

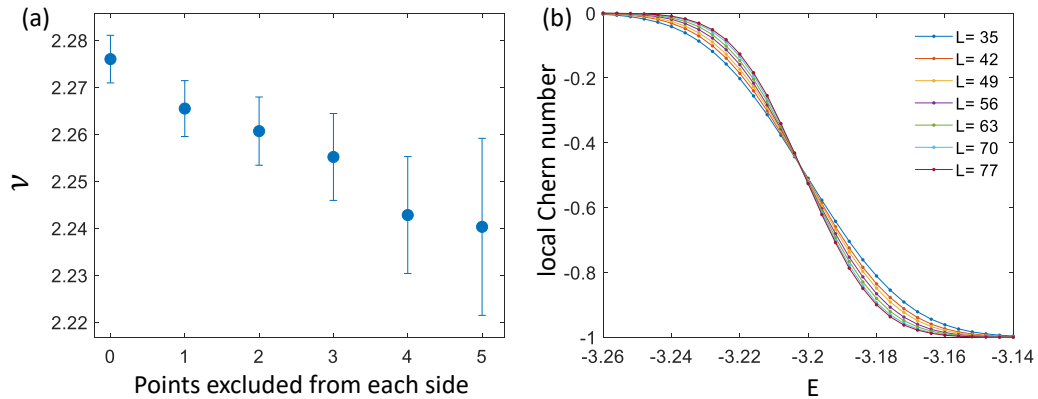


FIG. SF2. Determination of ν using method II in equilibrium: (a) Values of ν extracted from system sizes $L = 35, 42, \dots, 77$. The values on the horizontal axis denote the number of points that were excluded from both sides of E_c for each data set in panel (b). The critical energy was found to be $E_c \approx -3.2025$.

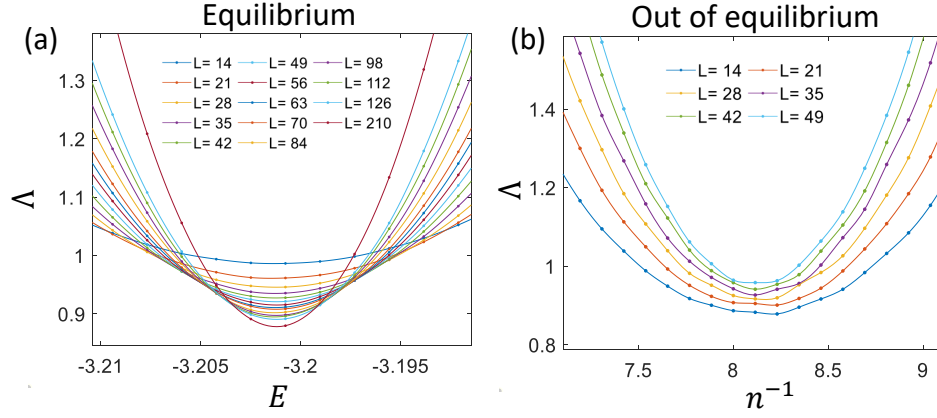


FIG. SF3. Dimensionless Lyapunov exponent (a) in and (b) out of equilibrium. The data presented here is the same as in Fig. 3 in the main text, but here we zoom in into the vicinity of E_c (n_c^{-1}). The need for corrections to scaling (even for the larger system sizes and even in equilibrium) is clearly evidenced by the variation of the minimal value of Λ with L .

corrections to scaling are significant even for larger systems sizes. Therefore, in order to obtain a good estimation for the critical exponent one should include irrelevant exponents in the scaling procedure. We will now present additional details regarding the corrections to scaling that were used in the fitting procedure in equilibrium. We assume the existence of only one irrelevant exponent (including more than a single irrelevant exponent would on the one hand be a numerical challenge which in general requires data with much lower uncertainties, and on the other hand seems not to be required in practice for the system sizes used). That is, we assume the following scaling form:

$$\frac{L}{\xi(E)} = f(u_r L^{1/\nu}, u_i L^{-y}), \quad (\text{S14})$$

where $\xi(E)$ is the localization length, f is some scaling function, u_r, u_i are the relevant and irrelevant scaling fields, respectively, and $y > 0$ is the irrelevant exponent. We can expand the scaling fields in the vicinity of E_c as $u_r(E - E_c) = \sum_{n=1}^{m_r} a_n (E - E_c)^n$, $u_i(E - E_c) = \sum_{n=0}^{m_i} b_n (E - E_c)^n$ (the term $n = 0$ is absent for the relevant field since it must vanish at the critical point). In addition, we expand f to the first order in the irrelevant field:

$$f(u_r L^{1/\nu}, u_i L^{-y}) \approx f_0(u_r L^{1/\nu}) + u_i L^{-y} f_1(u_r L^{1/\nu}), \quad (\text{S15})$$

where f_0, f_1 are some single-parameter functions. We will now present two approaches which lead to similar results:

(i) We assume a simple form of the scaling fields: $u_r(E) = E - E_c$, $u_i(E) = 1$, and take f_0, f_1 as the following polynomials: $f_0(x) = \sum_{n=0}^{n_1} a_n x^n$, $f_1(x) = \sum_{n=0}^{n_2} b_n x^n$, with $n_1 = 5, n_2 = 4$.

(ii) Following Ref. [47], we consider only even terms in the scaling functions: $f_0(x) = \sum_{n=0}^3 a_n x^{2n}$, $f_1(x) = \sum_{n=0}^2 b_n x^{2n}$, where $n_1 = 3, n_2 = 2$. However, we include additional terms in the expansion of the scaling fields: $u_r(E) = \sum_{n=1}^{m_1} c_n (E - E_c)^n$, $u_i(E) = \sum_{n=0}^{m_2} d_n (E - E_c)^n$, with $m_1 = 3, m_2 = 1$. This can be motivated by the fact that our data is close to being an even function around E_c , and the small asymmetry is reflected by the odd terms of the expansion of the scaling fields.

We have found both approaches to have low sensitivity to the choice of the smallest system size to be included in the fit, but are still somewhat affected by the range of energies taken around the critical energy E_c . As in method II, we chose a range of energies in which the result is most stable (least sensitive to increasing or decreasing the number of included points). We also verified that increasing n_1, n_2, m_1, m_2 has small impact on the results. A comparison of the results is presented in Fig. SF4. We have found approach (b) to be slightly more stable.

Out of equilibrium. We will provide here additional details regarding the transfer-matrix method and the choice of the parameters that were used to extract the localization length out of equilibrium. As described in the main text, we have calculated the matrix G^{-1} (of size $L_x \times L$, with periodic boundary conditions in both directions), for M different disorder realizations. We then set the hopping terms in G^{-1} with range along the x -direction larger than a cutoff p to be zero. Since the matrix now has only a *finite* hopping range, it is possible to extract the transfer-matrices by a straightforward generalization of the conventional nearest-neighbor case [70]: Suppose that we have a $L_x \times L$ Hamiltonian in a quasi-1D geometry with hopping range p in the x -direction. It can be written as $H = \sum_{r_x=1}^{L_x} \sum_{q=-p}^p H_{r_x, r_x+q}$, where H_{r_x, r_x+q} is the Hamiltonian describing hopping from slab r_x to slab $r_x + q$. We also define ψ_{r_x} as a length- L vector containing the wavefunction amplitudes associated with the r_x th slab. The

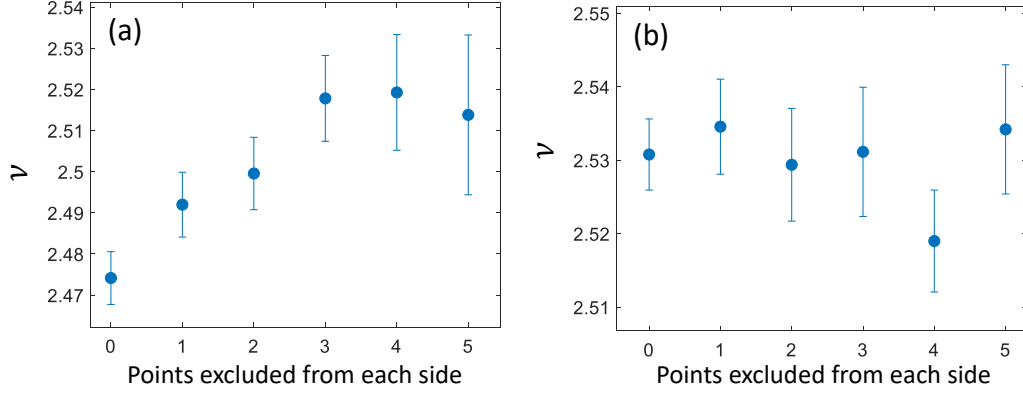


FIG. SF4. Values of ν extracted in equilibrium using method III and system sizes $L = 42, 49, 56, 63, 70, 84, 98, 112, 126, 210$. The values on the horizontal axis denote the number of points that were excluded from both sides of E_c for each data set in Fig. 3(a) of the main text. Panels (a) and (b) correspond, respectively, to approaches (a) and (b) described in the text.

eigenvalue equation can be written as: $\sum_{q=-p}^p H_{r_x, r_x+q} \psi_{r_x+q} = E \psi_{r_x}$ for each r_x , where E is the energy. We can isolate ψ_{r_x+p} and arrive to a recursion relation

$$\psi_{r_x+p} = (H_{r_x, r_x+p})^{-1} \cdot \left(E \psi_{r_x} - \sum_{q=-p}^{p-1} H_{r_x, r_x+q} \psi_{r_x+q} \right). \quad (\text{S16})$$

We can then define the transfer matrix T_{r_x} (of size $2pL \times 2pL$) as:

$$\begin{pmatrix} \psi_{r_x+p} \\ \vdots \\ \psi_{r_x-p+1} \end{pmatrix} = \begin{pmatrix} \dots & \dots & (\text{S16}) & \dots & \dots \\ \mathbb{I} & 0 & \dots & 0 & 0 \\ 0 & \mathbb{I} & \dots & 0 & 0 \\ \vdots & \vdots & \ddots & \vdots & \vdots \\ 0 & 0 & \dots & \mathbb{I} & 0 \end{pmatrix} \begin{pmatrix} \psi_{r_x+p-1} \\ \vdots \\ \psi_{r_x-p} \end{pmatrix} \equiv T_{r_x} \begin{pmatrix} \psi_{r_x+p-1} \\ \vdots \\ \psi_{r_x-p} \end{pmatrix}, \quad (\text{S17})$$

where in the first line appear the corresponding components of equation (S16), and \mathbb{I} is the $L \times L$ identity matrix.

Therefore, from each G^{-1} matrix we can extract $K = L_x - 2c$ transfer matrices, where $c = 7$ is a “safety margin”, which was chosen to be larger than p in order to avoid mixing between the first and the last transfer matrices of G^{-1} . The effective length would then be $L_{\text{eff}} = MK$. As for the choice of values for p and L_x , a priori it seems that the bigger L_x and p are, the smaller the resulting error (since the approximation becomes more accurate). While this is indeed the case for L_x , for p the situation is more subtle: To use Eq. (S16) we are required to calculate the inverse of H_{r_x, r_x+p} , which become exponentially small as p becomes larger. Therefore, p that is too large will lead to large numerical uncertainties in the inverse matrix.

In order to examine the effects of the value L_x on the calculation, we first set $p = 2$ [which is the exact hopping range of G^{-1} for the case of no disorder in the system Hamiltonian, see Eq. (5) of the main text] and investigate the dimensionless Lyapunov exponent Λ for different L_x , see Fig. SF5(a)–(c). We can see that $L_x = 105$ is already close to the limiting value. Then, we set $L_x = 105$ and investigate Λ for different values of p , see Fig. SF5(d)–(f). In addition, we have performed a calculation of the critical exponent for $L_x = 105$ and several values of p , and verified that $p = 4$ and $p = 5$ already give similar results. Based on this information, we chose $L_x = 105$ and $p = 5$ in the calculations that are presented in the main text.

As can be seen in Fig. SF3(b), corrections to scaling are needed to be accounted for also in the nonequilibrium case. However, since the effective L_x out of equilibrium is about 100-fold smaller than L_x in equilibrium (see Table I in the main text), the errors are about 10 times larger than in equilibrium. This prevents us from reliably including corrections to scaling in our fits. Therefore, we resolved to use the approach described in the main text, see in particular Fig. 3(d) there.

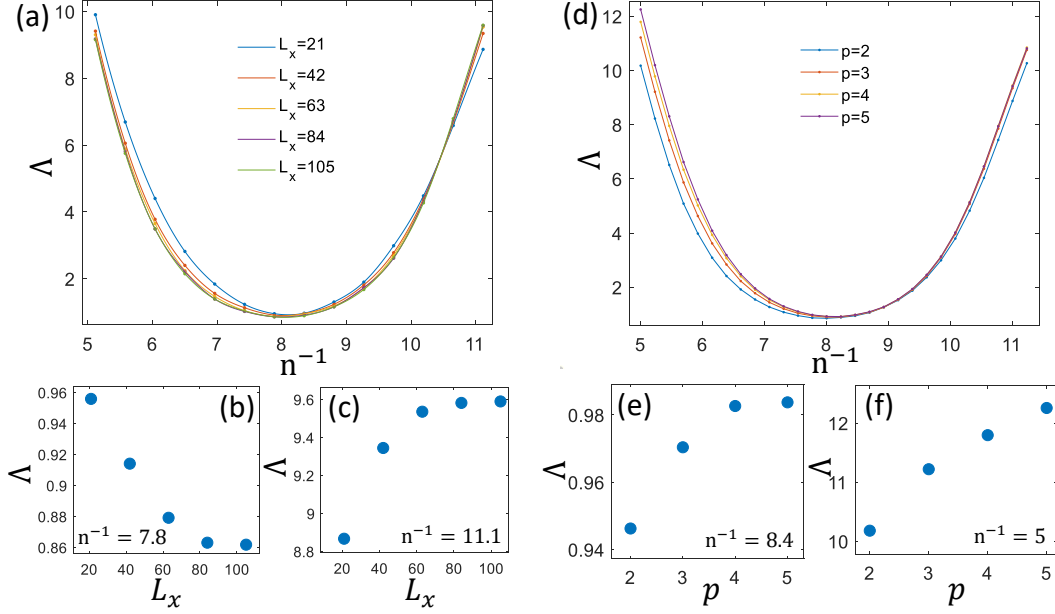


FIG. SF5. (a) the dimensionless Lyapunov exponent $\Lambda = \tilde{\Lambda}L = L/\xi$, Eq. (11) of the main text, as function of n^{-1} for $L = 28$, range cutoff $p = 2$, and different values of L_x (the size in the x -direction of the G^{-1} matrices). (b), (c) Λ as function of L_x , for two specific values of n^{-1} from panel (a). (d) Λ as function of n^{-1} for $L = 28$ and for different values of p (the range cutoff). (e), (f) Λ as function of p , for two specific values of n^{-1} from panel (d).

S.V. PARAMETER CHOICE AND UNIVERSALITY OF THE CRITICAL EXPONENT

In equilibrium, our model contains two parameters: (i) The dimensionless magnetic flux through a unit cell, $\alpha = Ba^2/\phi_0$, where $\phi_0 = h/e$ is the flux quantum and a is the lattice spacing; (ii) The onsite disorder strength W . These values should be chosen employing the following considerations [47]: (a) Unlike the continuum case, on the lattice each band of the Hofstadter model has an “intrinsic” width δ , the width of the band *without* disorder. Therefore, α should be chosen such that $\delta/\Delta \ll 1$, where Δ is the spacing between the Landau levels. However, a too small value of α is also not preferred since it would increase the magnetic length (measured in units of the lattice spacing a) $\ell_B = 1/\sqrt{2\pi\alpha}$, making the effective system size L/ℓ_B smaller (one can compensate for this by working with larger system sizes L , but it would be expensive in terms of computation time). (b) The disorder strength should be large enough such that the disorder-induced broadening of the band would be much larger than δ , but not as large as to mix between different Landau levels. If one picks the parameters following these considerations, one should obtain a universal value for the critical exponent, which is *independent* of the exact parameter values [47]. In our work, we have found $\alpha = 1/7$ and $W = 0.2$ to be appropriate in this respect.

Out of equilibrium instead of energy bands we have “occupation bands”, which are bands of eigenvalues n (occupations) of the single-particle density matrix G . Without disorder in H_S these bands are given by Eq. (5) in the main text. Our nonequilibrium model contains four parameters: (i) α of the reference Hamiltonian; (ii) W , the disorder strength in the system Hamiltonian H_S ; (iii) μ^{eff} , the effective chemical potential; (iv) γ^{in} , the refilling rate. We recall that we have proven in section S.I that if the system Hamiltonian H_S is zero then different values of μ^{eff} and γ^{in} will not affect the critical exponent (as long as μ^{eff} is not chosen near E_c , the critical energy of the band). While this proof does not hold for $W \neq 0$, if the parameters are chosen by similar considerations to those presented above for the equilibrium case, their exact values will not change the result, as we will show in what follows. In this work we have taken $\alpha = 1/7$, $\mu^{\text{eff}} = -3.6$ (that is, $E_c - \mu^{\text{eff}} \approx 0.4$, since $E_c \approx -3.2$), and $\gamma^{\text{in}} = 0.2$. For the disorder strength, we took $W = 2$ for Methods I and II. For Method III we chose $W = 5.5$, since it results in a more symmetric behavior around n_c , which somewhat reduces the need for corrections to scaling.

We will now present results which demonstrate that the critical exponent is indeed universal, in the sense of being insensitive to the exact parameter values. For concreteness we concentrate on Method II, though we have verified similar results hold for the other methods. We will separately change each one of the parameters while keeping the values of the rest the same. The results are plotted in Fig. SF6. In panels SF6(a-d) we compare the nonequilibrium scaling for different values of disorder W . We note that panel (b) corresponds to the same parameter values as in Fig. 2(b) in the main text, but also includes smaller system sizes. On the bottom panels we see the “occupation bands”,

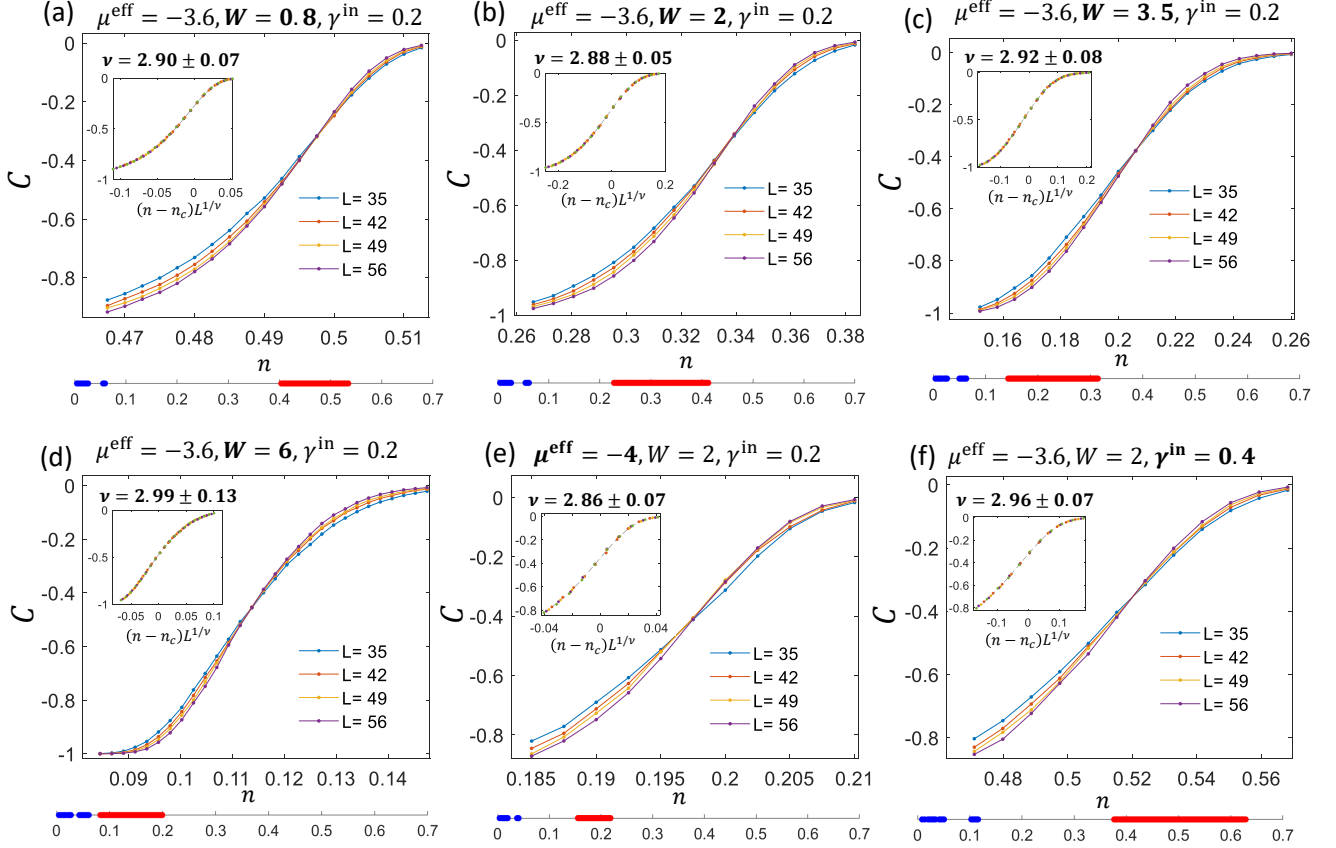


FIG. SF6. The average local Chern marker out of equilibrium, and the critical exponent extracted using Method II for different parameter values. Panels (a-d): $\mu^{\text{eff}} = -3.6, \gamma^{\text{in}} = 0.2$ and the disorder strength W takes different values. Panel (e): $\mu^{\text{eff}} = -4, W = 2, \gamma^{\text{in}} = 0.2$. Panel (f): $\mu^{\text{eff}} = -3.6, W = 2, \gamma^{\text{in}} = 0.4$. Insets: scaling data collapse. Bottom panel: the occupation bands. The critical exponent is seen to be universal, i.e., independent of the exact parameter values.

the spectrum of the single-particle reduced density matrix G , which are in the range of 0 to 1 (since they represent occupation values). The band that we investigate is the one with highest occupations [since it would correspond to the lowest energy band in equilibrium, or even out of equilibrium when the disorder is in the system-bath coupling Hamiltonian, cf. Eq. (5) of the main text], which is marked in red. We note that here there are also 7 bands as in equilibrium, but bands 3-7 have occupations that are close to zero and therefore hard to resolve in the figure. In panel SF6(e) we take $\mu^{\text{eff}} = -4$, which doubles the value of $E_c - \mu^{\text{eff}}$ from 0.4 to 0.8. In panel SF6(f) we take $\gamma^{\text{in}} = 0.4$ instead of 0.2. It is evident that while each different parameter choice leads to a change in the position and shape of the highest-occupancy band, all of the cases result in a similar value of $\nu \sim 2.9$, agreeing with the result presented in the main text, and demonstrating their universality.

S.VI. DISTRIBUTION OF G^{-1}

As discussed in the main text, out of equilibrium the steady state single-particle density matrix matrix G plays the role of the Hamiltonian in characterizing both the topology of the system and its localization properties. In that respect, concentrating on its inverse G^{-1} offers some advantages. This is particularly clear if $H_S = 0$, that is, in the clean case or if disorder is included only in the reference Hamiltonian, since then G^{-1} is simply related to h^{ref} via Eq. (5) of the main text. This implies that G^{-1} and h^{ref} share the same eigenvectors, and moreover, that for nearest neighbor h^{ref} , G^{-1} has up to next-nearest neighbor terms ($p = 2$), which allows its study via the transfer matrix without approximation with respect to the range. However, as was mentioned in the main text, this is no longer the case when the disorder is included in the system Hamiltonian; now in order to obtain G^{-1} one needs to solve numerically the continuous Lyapunov equation, Eq. (3) of the main text. Therefore, we will now study its statistical properties in this case.

Fig. SF7(a)-(b) presents: (i) The distribution of the absolute values of onsite terms of the matrix G^{-1} , i.e., the diagonal terms $(G^{-1})_{ii}$ where $i = (r_x, r_y)$; (ii) The distribution of the absolute values of terms connecting sites along

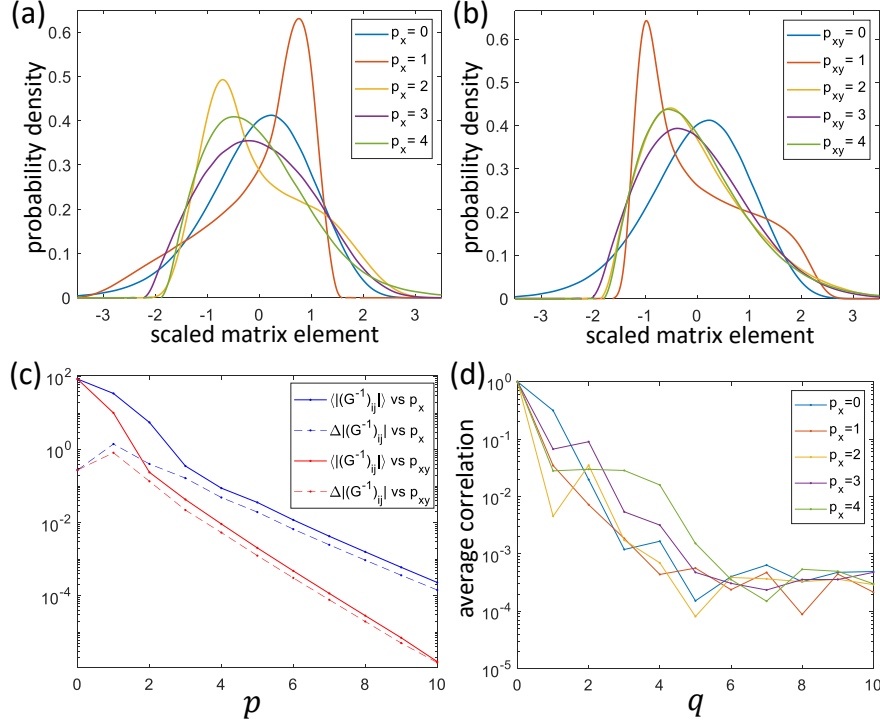


FIG. SF7. (a) The distributions of absolute values of the matrix elements $(G^{-1})_{ij}$ connecting sites along the x -direction, where $i = (r_x, r_y)$ and $j = (r_x + p_x, r_y)$ with $p_x = 0, \dots, 4$ ($p_x = 0$ is the onsite term), shifted by their respective expectation values and normalized by their respective standard deviations. (b) The distributions of the absolute values of the matrix elements of $(G^{-1})_{ij}$ connecting sites along the $\pi/4$ diagonal in the xy -plane, where $i = (r_x, r_y)$ and $j = (r_x + p_{xy}, r_y + p_{xy})$ with $p_{xy} = 0, \dots, 4$ ($p_{xy} = 0$ is the onsite term), shifted by their respective expectation values and normalized by their respective standard deviations. (c) Semi-log plot of the expectation values and standard deviations of the absolute values of the elements $(G^{-1})_{ij}$ connecting sites along the x -direction (blue), and connecting sites along the $\pi/4$ diagonal in the xy -plane (red). (d) Semi-log plot of the correlation $\mathcal{C}_{p_x}(q)$ [Eq. (S18), normalized by its value at $q = 0$] of the absolute values of matrix elements $(G^{-1})_{ij}$ connecting sites along the x -direction with $p_x = 0, \dots, 4$. q is the distance between the correlated terms (along either the x - or the y -direction). For the calculations, $M = 2000$ realizations of G^{-1} were generated, each with $L_x = 105$, $L_y = 28$ (with periodic boundary conditions), $\gamma^{\text{in}} = 0.2\gamma^0$, $\mu^{\text{eff}} = -3.6$, and disorder strength $W = 5.5$.

the x -direction, i.e., off-diagonal terms $(G^{-1})_{ij}$ with $i = (r_x, r_y)$ and $j = (r_x + p_x, r_y)$ (similar distributions are obtained for sites separated along the y -direction); (iii) The distribution of the absolute values of terms connecting sites along the $\pi/4$ diagonal in the xy -plane, i.e., the off-diagonal terms $(G^{-1})_{ij}$ with $i = (r_x, r_y)$ and $j = (r_x + p_{xy}, r_y + p_{xy})$. The distributions (ii) and (iii) are shown, respectively, in panels (a) and (b); the onsite term (i) appears in both panels as the term $p_x = 0$ and $p_{xy} = 0$, respectively. The distributions are shifted by their respective expectation values and normalized by their respective standard deviations, which are presented in panel (c). In panel (d), we can see the average correlation of the absolute values of the matrix elements of G^{-1} which connect sites along the x -direction. The correlation is defined as:

$$\mathcal{C}_{p_x}(q) = \left\langle \left| (G^{-1})_{i_1 i_2} \right| \left| (G^{-1})_{j_1 j_2} \right| \right\rangle - \left\langle \left| (G^{-1})_{i_1 i_2} \right| \right\rangle \left\langle \left| (G^{-1})_{j_1 j_2} \right| \right\rangle, \quad (\text{S18})$$

where $i_1 = (r_x, r_y)$, $i_2 = (r_x + p_x, r_y)$, and where j_1 and j_2 are shifted with respect to i_1 and i_2 by q sites along either the x -direction [$j_1 = i_1 + (q, 0)$, $j_2 = i_2 + (q, 0)$] or the y -direction [$j_1 = i_1 + (0, q)$, $j_2 = i_2 + (0, q)$] — both options gave similar results, and we averaged over them to reduce statistical noise. The correlation is normalized by its value at $q = 0$ (the variance), which can be inferred from the standard deviations plotted in panel (c).

An important observation is that the distributions do not feature any long tails. Moreover, Fig. SF7(c) shows that both the expectation values and standard deviations of the various terms decay exponentially with range (p_x or p_{xy}). And Fig. SF7(d) demonstrates that the same is true for the correlations between different elements (the saturation at $q > 6$ is due to the values becoming smaller than the statistical error). This justifies cutting off the range, as done in the transfer matrix method III out of equilibrium. Moreover, as notes in the main text, the new localization universality class we find cannot be attributed to G^{-1} having terms with long range or fat-tailed distributions, and

therefore seems to be a genuine nonequilibrium effect.

Finally, a curious fact is that one can derive an analytic result for the expectation value of the onsite terms. Starting from the continuous Lyapunov equation [Eq. (3) of the main text], we can multiply by G^{-1} from the right and then take the trace, leading to

$$\gamma^{\text{in}} \text{Tr}(G^{-1}) = \text{Tr}(\gamma^{\text{in}} + \gamma^{\text{out}}), \quad (\text{S19})$$

independently of h_S^* . Taking h^{ref} to be the Hofstadter Hamiltonian [Eq. (4) of the main text], we can see that $\text{Tr}(h^{\text{ref}}) = 0$ and $\text{Tr}((h^{\text{ref}})^2) = 4L_x L_y$. Substituting $\gamma^{\text{out}} = \gamma^0 (h^{\text{ref}} - \mu^{\text{eff}})^2$, this results in

$$\langle (G^{-1})_{ii} \rangle = 1 + \frac{1}{\gamma^{\text{in}}} (4 + \mu^{*2}), \quad (\text{S20})$$

since $\langle (G^{-1})_{ii} \rangle$ is independent of i (for periodic boundary conditions), and hence equals $\text{Tr}(G^{-1})/L_x L_y$. Eq. (S20) shows that the onsite average depends only on γ^{in} and μ^{eff} , but is independent of the disorder strength W ; this would no longer be true for the corresponding standard deviation.
